Water Reactor Safety Research

Heat Transfer Highlights

February 1979

Reactor Analysis and Safety Division
ARGONNE NATIONAL LABORATORY
9700 South Cass Avenue
Argonne, Illinois 60439

RSR Monthly Progress Report

Transient Critical Heat Flux

1. Local Conditions in Blowdown Experiments (J.C.M. Leung and R.E. Henry)

A detailed local condition analysis of the heated core requires specifying boundary conditions at both ends (inlet and outlet) of the core as well as heat flux at the heater wall surface. For example, in the Semiscale MOD-1 core, Varacalle, et al., have obtained local conditions for S-02-9 using RELAP4 core model by specifying pressure and enthalpy at the upper plenum boundary, and mass flow and enthalpy at the inlet core mixer box[1],[2] (which houses the turbine flowmeter, drag disc and gamma densitometer). The surface heat flux is obtained via an inverse heat conduction technique[3] by inputting the local power generation rate and the measured temperature just behind the outer sheath of the heater. Unfortunately, the mass flowrate at the core inlet was not measured accurately early in the transient; the response of the inlet flowmeter was too slow and the drag disc reached its mechanical limit between 0.1 and 0.3 sec.[2] Furthermore, there are uncertainties in the calculated heat flux as a result of variations (just to name a few) in the location of thermocouples, porosity of boron nitride and gap conductance. These types of variations are being analyzed in the heaters of THTF bundle (ORNL) by a very long calibration procedure.[4],[5] The lack of mass flow and density measurements in the THTF core prevents a detailed local condition calculation just within the core itself. An alternative is to use the core pressure drop information but the DP cell output exhibited prolonged ringing signals which are exceedingly difficult to make use of.[6] The local condition analyses had been performed so far using the spool piece measurements (pressure, mass flow and density) outside the core. Once again the difficulties encountered in the turbine flowmeter and drag disc were reported[7] and therefore the uncertainty in the local

fluid conditions cannot be quantified during the first 1.5 sec (Test 105).[6] This is unfortunate since most of the heater thermocouples indicated CHF within this time.

In the single-tube Freon blowdown experiments, the simple geometry together with the accurate measurement of pressures, temperatures, and mass flow should lend itself to a more reliable local fluid condition analysis. A new uniform-flux test section which has 20 three-wire thermocouples[8] installed on the outer wall has been fabricated. The three-wire thermocouple measures the actual outer wall temperature while eliminating the IR drop voltage pickup caused by dc heating. The test section is insulated by more than 1/2 in. of ceramic fiber insulation and a couple of thermocouples have been installed to measure the insulator response during the transient. The mass flowrate at the inlet break will constitute one boundary condition and hence accurate prediction of choked flowrate is essential, particularly in the subcooled and near-saturated regime. Preliminary steady-state results show that the Henry-Fauske critical flow model prediction is in good agreement with the measurements over a wide range of subcooling and stagnation pressure in Freon-11 as shown in Fig. 1. The mathematical tool necessary for the local condition analysis is outlined in the next section.

2. Analytical Support for Transient CHF (J.C.M.Leung and K. Gallivan)

A one-dimensional transient coolant dynamics model which bears some resemblance to SAS1A[9] (ANL) and BACTRAC[10] (MIT) was proposed.[11] This model considers an incompressible liquid and a compressible two-phase mixture. The use of two-step Lax-Wendroff explicit scheme[12] in the solution of two-phase compressible region was found to require excessive computer time since the numerical stability is dictated by the Courant's criterion,

$$\Delta t \leq \frac{\Delta z}{c + |u_{max}|} \tag{1}$$

where Δt, Δz, c, and u_{max} are respectively the time step, node spacing, acoustic velocity and the maximum fluid velocity. For a node spacing of 2 in., the allowable time step is about 1 msec or less since c is an order of magnitude larger than u_{max}. A new scheme is proposed here which relaxes the constraint given in Eq. 1 to

$$\Delta t \leq \frac{\Delta z}{|u_{max}|} \tag{2}$$

which means the time step be such that no fluid particle is allowed to traverse more than one node spacing. This results in significant saving in computation time as will be demonstrated later. Essentially this scheme neglects the acoustic phenomena (or pressure wave propagation) as first suggested by Meyers.[13] This is accomplished by assuming that density (ρ) can be evaluated as a function of enthalpy (h) only,

$$\rho = \rho(h) \tag{3}$$

which applies therefore to both single-phase liquid and two-phase. Essentially this assumption decouples the momentum equation from the continuity and energy equations. For a pressure-driven boundary condition (i.e., given test-section pressure drop ΔP), an integrated momentum equation is employed as suggested by Meyers[13]:

$$\frac{d\bar{G}}{dt} = \frac{1}{L}(\Delta P - F) \tag{4}$$

where

$$\bar{G} = \text{ave mass velocity} = \frac{1}{L}\int_0^L G\, dz$$

and the total resistance to fluid flow F, is given by

$$F = \left(\frac{G^2}{\rho}\right)_{out} - \left(\frac{G^2}{\rho}\right)_{in} + \int_o^L \frac{2f}{D\rho} G|G| dz + \int_o^L \rho g \, dz \tag{5}$$

The continuity and energy equations are written as

$$\frac{\partial \rho}{\partial t} + \frac{\partial G}{\partial z} = 0 \tag{6}$$

$$\frac{\partial h}{\partial t} + \frac{G}{\rho} \frac{\partial h}{\partial z} = \frac{\phi P_h}{\rho A_x} + \frac{1}{\rho} \frac{\partial P}{\partial t} \tag{7}$$

where P_h and A_x are the heated perimeter and flow area, respectively. The combination of the continuity and energy equations has been shown to describe the local rates of fluid expansion in single phase and voiding in two-phase.[14] In two-phase, the particular result is

$$\frac{\partial u}{\partial z} = \underbrace{\frac{\phi P_h v_{fg}}{A_x h_{fg}}}_{I} + \underbrace{\frac{v_{fg}}{h_{fg}} \left[1 - \frac{1}{v}\left(\frac{\partial h}{\partial P}\right)_x\right] \frac{dP}{dt}}_{II} \tag{8}$$

It can be seen that the volumetric flux variation of the two-phase mixture depends on the (I) wall heat flux ϕ and (II) flashing as a result of depressurization. The step-by-step solution method of Eqs. 6 and 7 is too long to be reported here but basically the finite difference form of the equations was integrated in stepwise manner using a predictor-corrector scheme.

A test problem was examined using both the compressible scheme, (i.e., Lax-Wendroff method) and the present scheme which neglects the sonic phenomena. A tube of length 128 in. initially filled with Freon mixture of x = 0.1 was subjected to a rapid exponential pressure decay without heat addition as shown in Fig. 2,

$$P_1 = 300 - 20\ (1 - e^{-t})\ \text{psia} \qquad (9)$$

$$P_2 = 297.3 - 17(1 - e^{-t})\ \text{psia} \qquad (10)$$

where P_1 and P_2 are the prescribed inlet and exit pressure, respectively. The predicted exit and inlet velocities are shown in Figs. 2 and 3 respectively for the two schemes employed. The two methods exhibit remarkably good agreement; the present scheme is seen to smooth out the high frequency oscillation in velocities which are predicted by the compressible scheme. The oscillation is felt to be the result of the pressure wave propagation phenomena which has a transport time of 0.09 sec in the test section. After 2 sec the velocity oscillations were damped out sufficiently so that the two schemes predict identical results from then on. The 4 sec transient requires 120 CPU secs for the compressible solution and only 7 CPU sec for the present solution.

Version 1 of the present scheme which has been completed handles a prescribed wall heat flux and pressure driven boundary at both ends. An actual isothermal blowdown (here meaning no power input) has been analyzed using this present version. The heat flux to the coolant during blowdown was calculated via a simple heat balance which assumes the wall temperature to follow saturation.[14] The pressure boundary values were obtained using the experimental pressure at the top and the test-section DP cell. However early in the blowdown (~1 sec) excessive ringing in DP cell output was observed and an electronic filter wqs used to damp out the oscillation and therefore the results would not be reflecting the early thermal-hydraulic of the system. The predicted velocities are compared to the turbine flowmeter measurements in Fig. 4. The velocity at the top (TV2) was predicted rather well but the velocity at the bottom (TV1) was underpredicted in magnitude by the present scheme. This discrepancy

could be caused by the conservatism in the heat flux boundary evaluation which did not take into account the stored heat in the insulation. If more heat was to be extracted by the coolant, a higher voiding rate which led to a higher velocity would be expected. This preliminary result is particularly encouraging in view of the fact that COBRA-IV-I [5] yields a less satisfactory comparison as shown in Fig. 5.

Version 2 is at present being implemented to handle flow-driven boundary condition at one end. This couples with a critical flow prediction at the break will enable a separate evaluation of local conditions.

References

1. D. J. Varacalle, "Preliminary RELAP4 Studies of the 1-1/2 Loop MOD-1 Semiscale Facility for Utilization in Local Conditions Development of the Heat Transfer Data Bank," PG-R-77-19 (July 1977).

2. D. J. Varacalle et al., "Local Conditions and Uncertainty Band Calculations for Semiscale Test S-02-9," CDAP-TR-048 (Jan 1979).

3. D. M. Snider, "INVERT--A Program for Solving the Non-Linear Inverse Heat Conduction Problem for One-Dimensional Solids," TREE-NUREG-1119 (to be published).

4. L. J. Ott and R. A. Hedrick "ORTCAL--A Code for THTF Heater Rod Thermocouple Calibration," ORNL/NUREG-51 (Feb 1979).

5. L. J. Ott and R. A. Hedrick, "ORINC--A One-Dimensional Implicit Approach to the Inverse Heat Conduction Problem," ORNL/NUREG-23 (Nov 1977).

6. W. G. Craddick et al., "PWR Blowdown Heat Transfer Separate-Effects Program Data Evaluation Report-Heat Transfer for THTF Test Series 100," ORNL/NUREG-45 (1978).

7. R. A. Hedrick et al., "PWR Blowdown Heat Transfer Separate-Effects Program Data Evaluation Report-System Response for THTF Test Series 100," ORNL/NUREG-19 (1977).

8. D. Henkel, "Measurement of Surface Temperature at DC Heated Channels by Three-Wire Thermocouples," MAN Rpt. No. 09.32.01 (Nov 1963).

9. J. C. Carter et al., "SAS1A, A Computer Code for the Analysis of Fast Reactor Power and Flow Transients," ANL-7607 (1970).

10. R. A. Smith, "Critical Heat Flux in Flow Reversal Transients," Ph.D. Thesis, ME Dept., MIT (1975), also EPRI NP-151 (May 1976).

11. J.C.M. Leung and K. Gallivan, "Analytical Support for Transient CHF," Water Reactor Safety Research Monthly Progress Report for July 1978, Argonne National Laboratory (Aug 1978).

12. R. D. Richtmyer and K. W. Morton, Difference Methods for Initial-Value Problems, Interscience Publishers, Second ed (1967).

13. J. E. Meyers, "Hydrodynamic Models for the Treatment of Reactor Thermal Transients," Nucl. Sci. Eng., 10, p. 269 (1961).

14. J.C.M. Leung and R. E. Henry, "Transient Critical Heat Flux," Water Reactor Safety Research Monthly Progress Report for Nov 1978, Argonne National Laboratory (Jan 1979).

15. C. L. Wheeler et al., "COBRA-IV-I: An Interim Version of COBRA for Thermal Hydraulic Analysis of Rod Bundle Nuclear Fuel Elements and Cores," BNWL-1962 (1976).

3.10.79

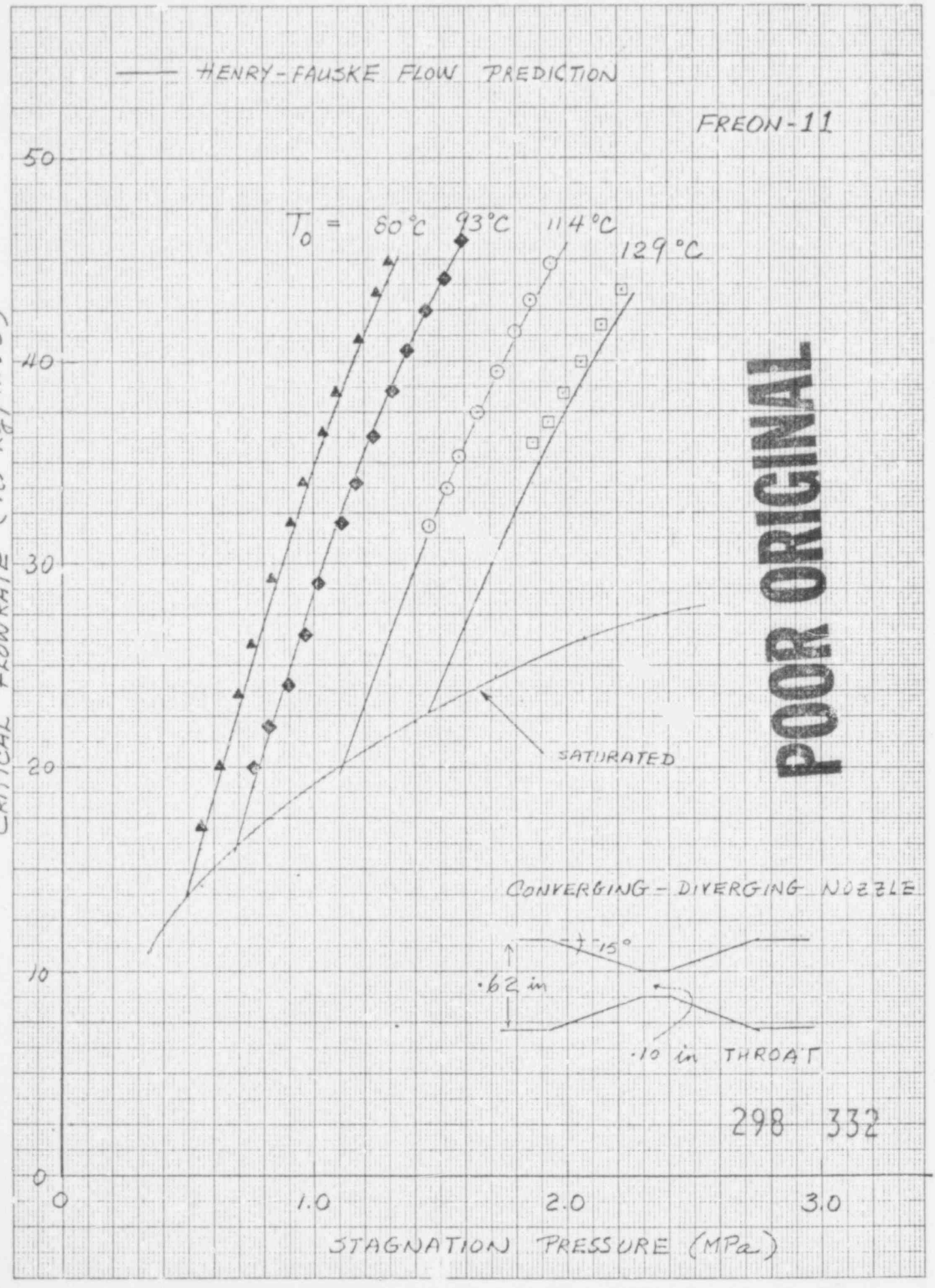

Fig. 1. Henry-Fauske Prediction of Subcooled Critical Flow Data in Nozzle.

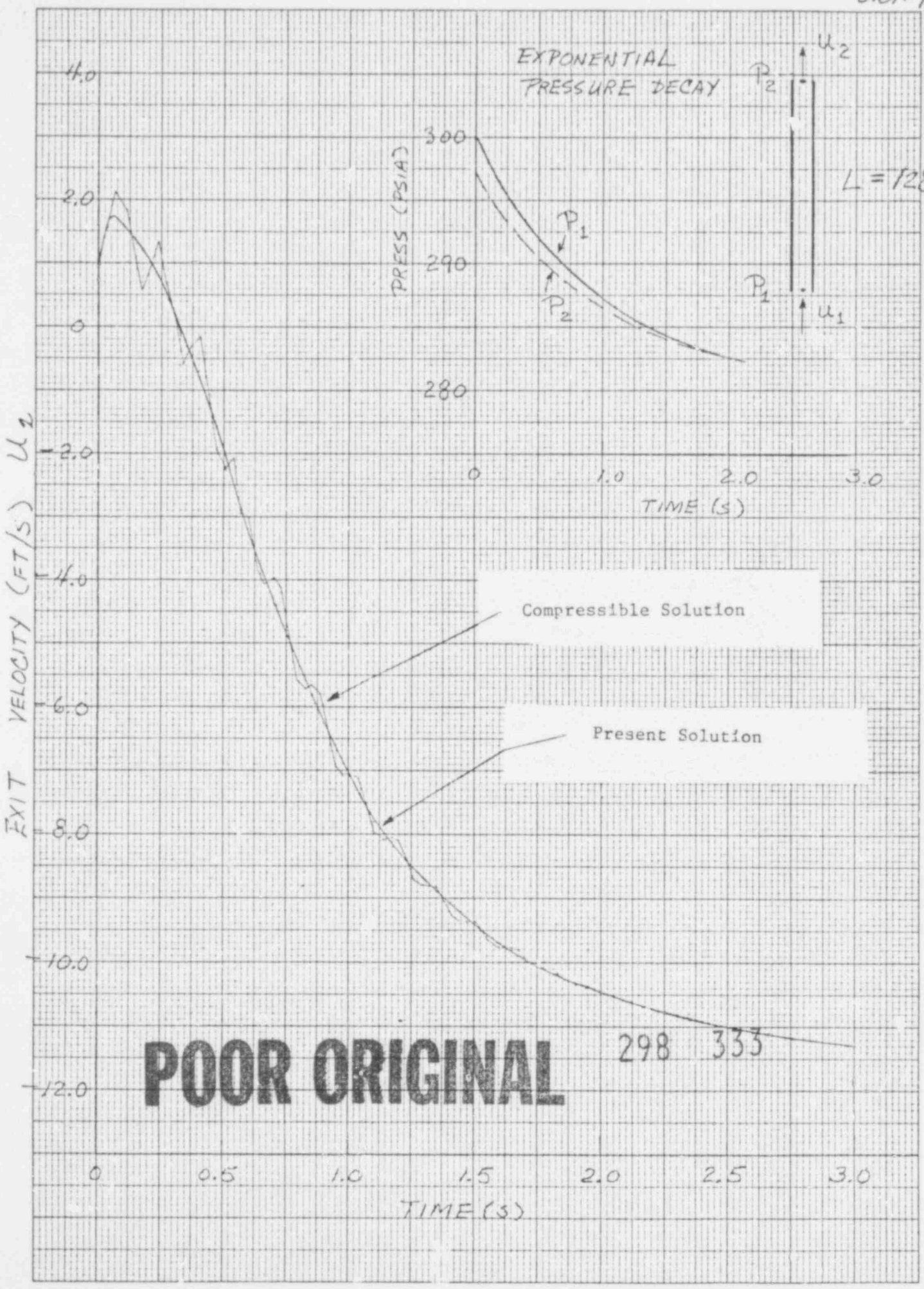

Fig. 2. Exit Velocity Comparison During Exponential Pressure Decay Test Problem.

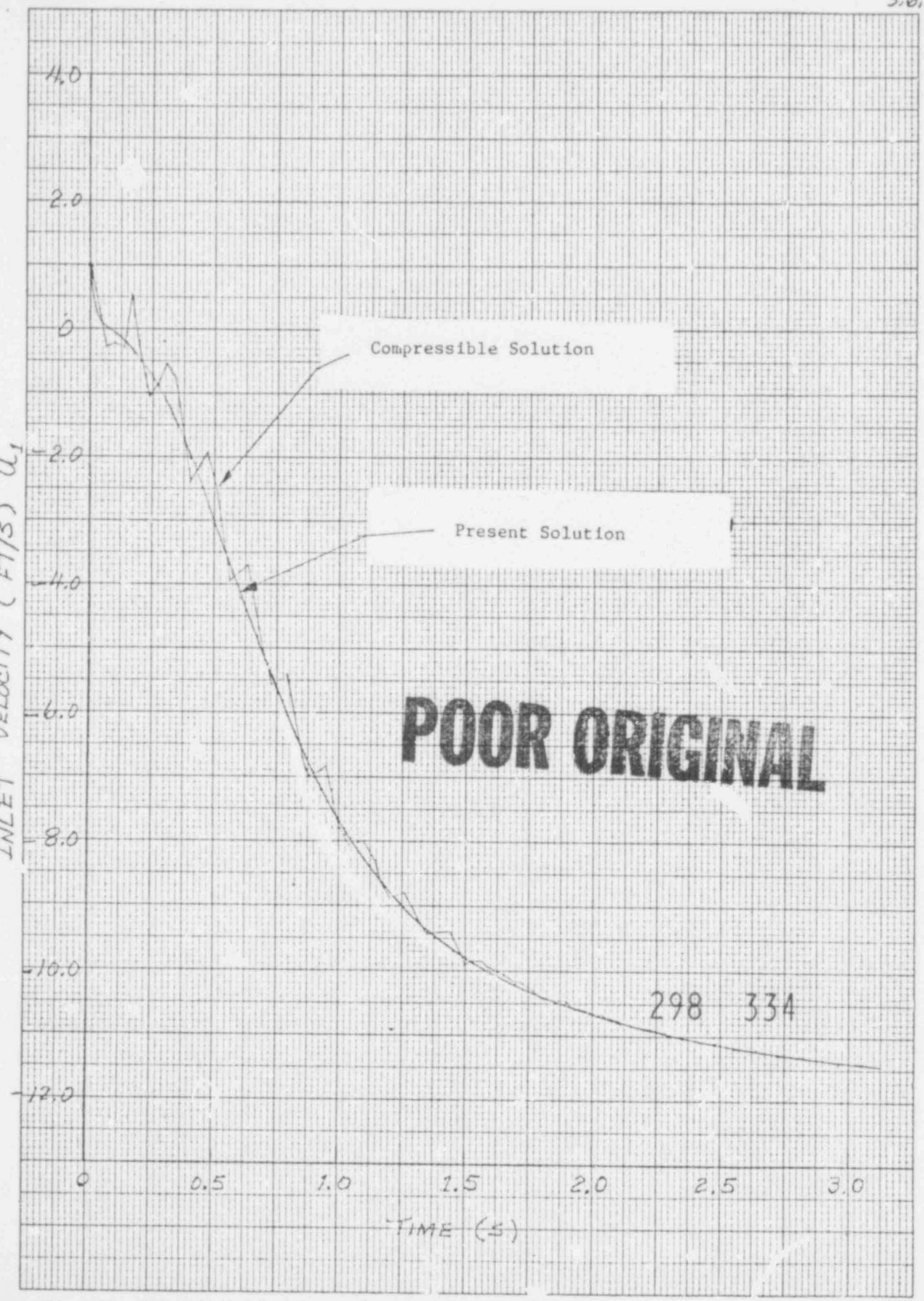

Fig. 3. Inlet Velocity Comparison During Exponential Pressure Decay Test Problem.

Fig. 4. Comparison of Present Scheme Prediction with Inlet and Exit Turbine Velocity Measurement.

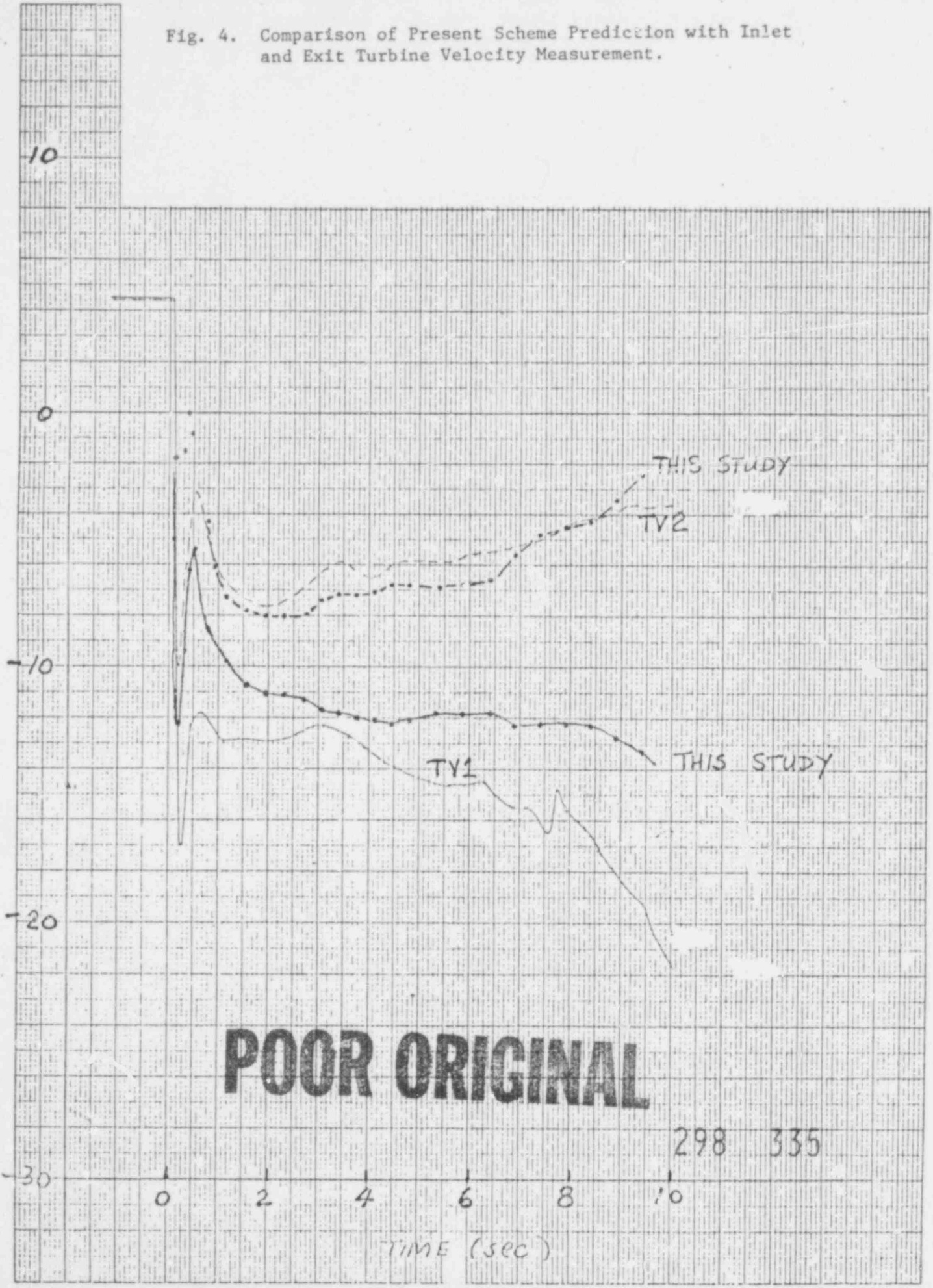

Fig. 5. Comparison of COBRA-IV-I Prediction with Inlet and Exit Turbine Velocity Measurement.

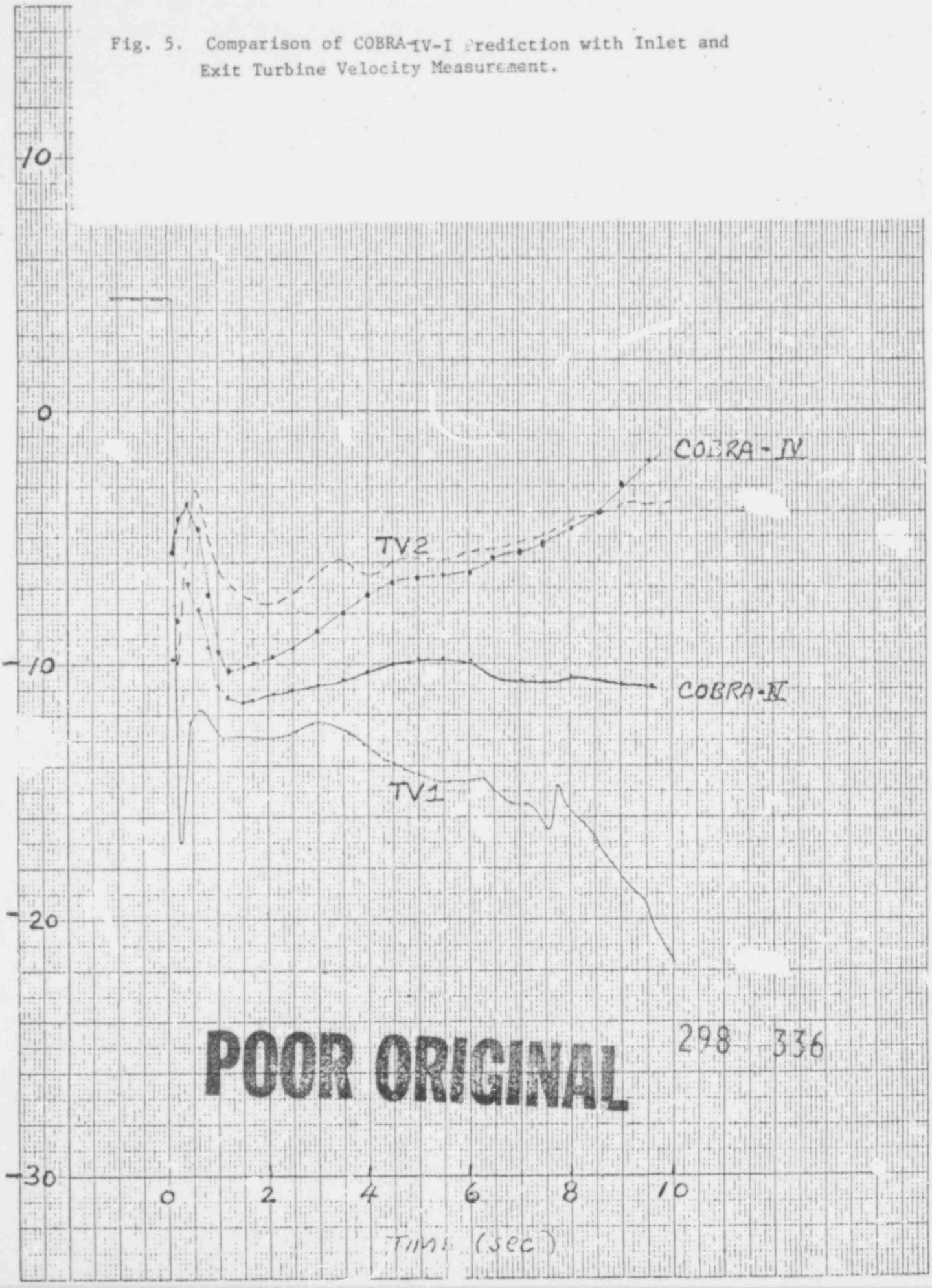

Monthly Progress Report

Reflood Tests (Y. S. Cha, R. E. Henry, P. A. Lottes)

Several tests were performed with relatively low average inlet velocities (∿2.5 cm/s) and with a subcooling of ∿7°C for the inlet fluid (all previous tests were performed with an inlet subcooling of ∿35°C). The operating conditions and the measured results are shown in Table I, where

$T_{18,i}$ = initial temperature of thermocouple No. 18.

f = frequency of forced-oscillation.

β_f = opening position of the throttle valve between the supply tank and the test section.

β_r = opening position of the throttle valve between the receiving tank and the test section.

P_s = pressure in the supply tank.

P_r = pressure in the receiving tank.

T_i = inlet water temperature.

T_d = temperature at the discharge end of the test section.

Δl_f = change in liquid level in the supply tank.

Δl_r = change in liquid level in the reverse tank.

Δl_e = change in liquid level in the recirculation tank.

Δt = time required to complete a test.

$\bar{V}_i$ = inlet average velocity to the test section.

$\bar{V}_f$ = average velocity during forward flow.

$\bar{V}_r$ = average velocity during reverse flow.

$\bar{V}_i = (\bar{V}_f - \bar{V}_r)/2$

d_f = orifice diameter for forward flow.

d_r = orifice diameter for reverse flow.

Comparisons of the results of quench time versus axial distance for Run No. 59, 61, 63, and 66 are shown in Fig. 1. It is seen that the quench front velocity increases with increasing frequency of oscillation. This result is consistent with the results reported previously with approximately the same inlet average velocity but with an inlet subcooling of 35°C. It can be observed from Fig. 1 that the difference in quench time at the same axial location is small between tests with f = 2.80 H_z and f = 1.0 H_z and test without forced-oscillation. There is a relatively large difference in quench time between test with f = 0.26 H_z and tests with other frequency of oscillation. The largest difference in quench time appeared near the ends of the tests (at an axial distance of 2.13m) and the difference is approximately 25%.

Figure 2 shows the comparisons between tests with different inlet subcoolings. Run No. 53, 54, 62, and 65 all have an inlet average velocity of approximately 2.5 cm/s. Run No. 53 has an inlet subcooling of 35°C with f = 1.11 H_z. Run No. 54 has an inlet subcooling of 35°C with f = 2.78 H_z. It can be observed from Fig. 2 that the difference in quench time is small between tests with different inlet subcoolings.

Run No.	$T_{18,i}$ (°C)	f (Hz)	β_f (turns)	β_r (turns)	P_s (MPa)	P_r (MPa)	Power (kw)	T_i (°C)	T_d (°C)	Δl_f (cm)	Δl_r (cm)	Δl_e (cm)	Δt (sec)	$\bar{V}_i$ (cm/s)	$\bar{V}_f$ (cm/s)	$\bar{V}_r$ (cm/s)	$\bar{V}_r/\bar{V}_f$	d_f (cm)	d_r (cm)
59	705	0	1.20	-	0.411	-	0	93	121	19.4	0	7.8	424	2.89	2.89	0	0		0.381
60	707	0.26	3.0	-	0.411	0.101	0	93	121	38.7	24.1	4.8	395	2.33	12.5	7.8	0.62		0.381
61	705	0.26	3.3	-	0.411	0.101	0	93	121	42.2	24.1	7.6	390	2.94	13.8	7.9	0.57		0.381
62	709	0.98	3.0	-	0.411	0.091	0	93	121	39.5	24.1	4.4	390	2.49	12.9	7.9	0.61		0.381
63	699	1.01	3.3	-	0.411	0.095	0	93	121	40.2	23.6	5.9	366	2.85	14.0	8.3	0.59		0.381
64	705	0.98	3.3	-	0.411	0.101	0	93	121	43.0	22.7	8.4	402	3.20	13.6	7.2	0.53		0.381
65	708	2.78	3.0	-	0.411	0.079	0	93	121	39.5	24.8	6.7	372	2.50	13.5	8.5	0.63		0.381
66	711	2.80	3.0	-	0.411	0.081	0	93	121	41.3	23.7	7.0	385	2.90	13.7	7.9	0.58		0.381
67	705	2.73	3.0	-	0.411	0.090	0	93	121	36.0	17.1	8.6	353	3.39	13.0	6.2	0.48		0.381

TABLE I

Operating Conditions and Measured Results for Run No. 59 through 67.

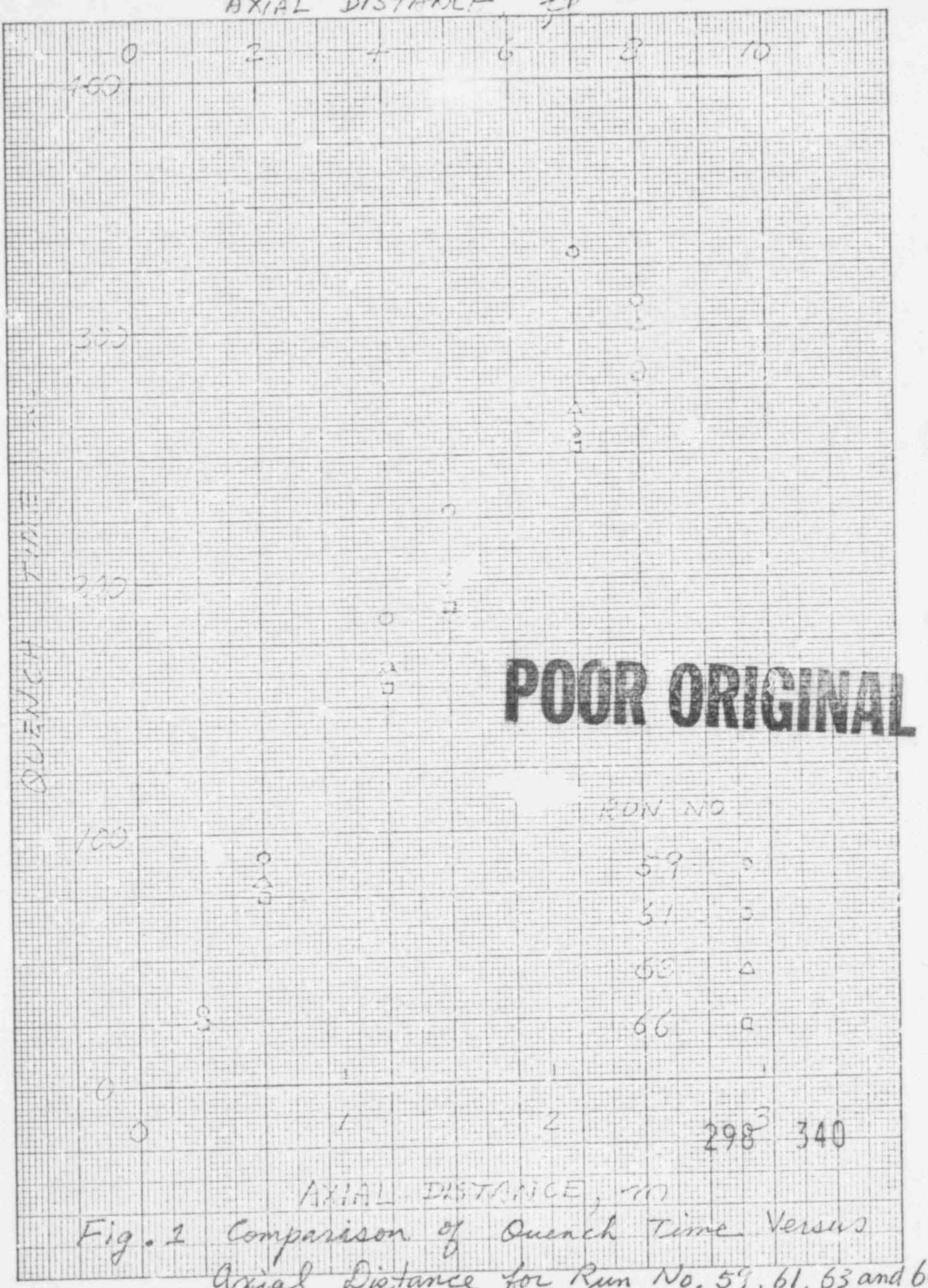

Fig. 1 Comparison of Quench Time Versus Axial Distance for Run No. 59, 61, 63 and 66.

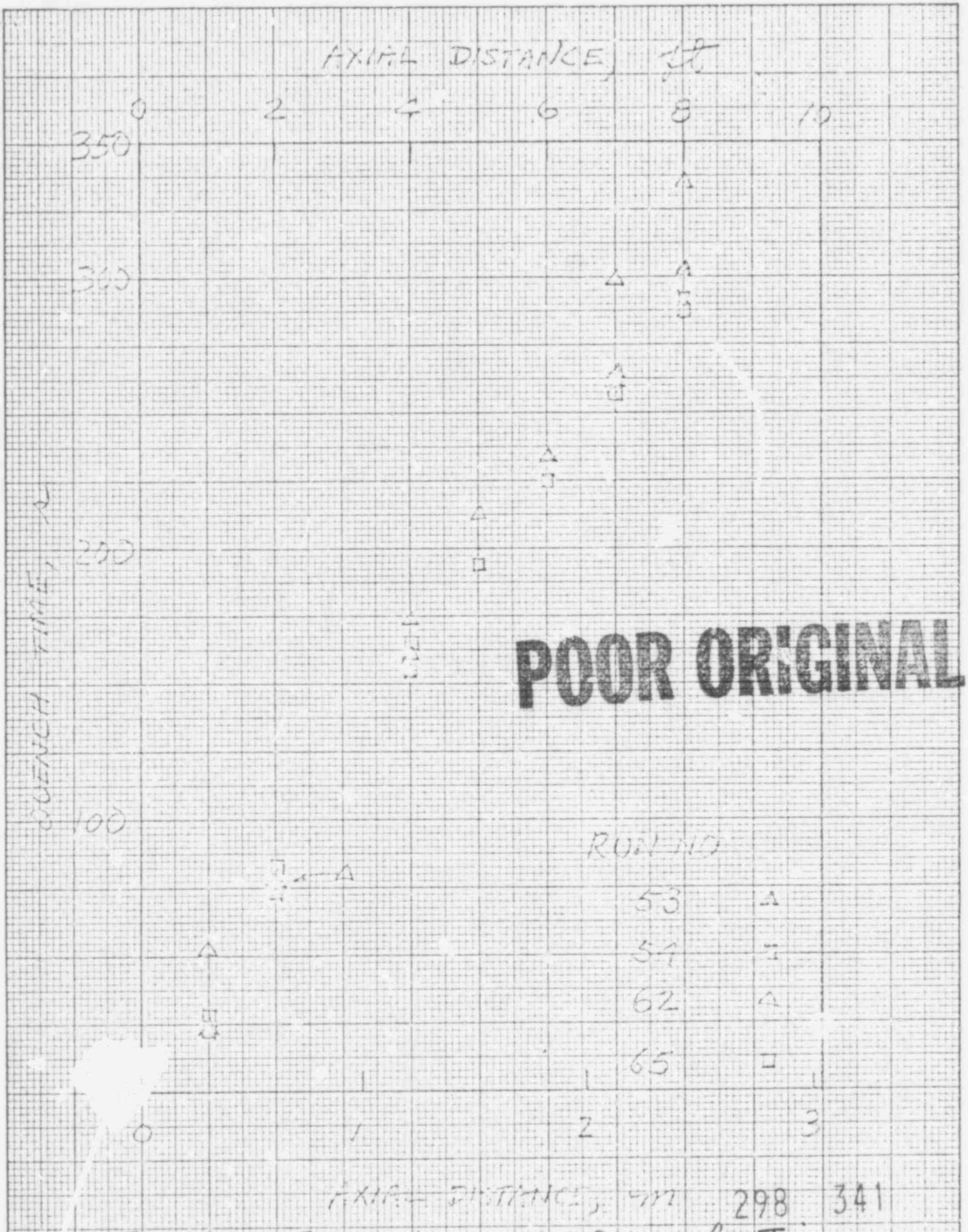

Fig. 2 Comparison of Quench Time Versus Axial Distance for Tests with Different Inlet Subcoolings.